High Temperatures-High Pressures, Vol. 52, pp. 263–283
Reprints available directly from the publisher
Photocopying permitted by license only
DOI: 10.32908/hthp.v52.1423

Normal spectral emissivity and heat capacity of Pd–Fe melts measured at constant pressure under electromagnetic levitation with a static magnetic field

Manabu Watanabe[1]*, Masayoshi Adachi[2],
Masahito Uchikoshi[2] and Hiroyuki Fukuyama[2]*

[1]*Department of Materials Science and Engineering, Tokyo Institute of Technology, Yokohama 226-8502, Japan*
[2]*Institute of Multidisciplinary Research for Advanced Materials, Tohoku University, Sendai 980-8577, Japan*

Received: January 6, 2023; Accepted: February 20, 2023.

The normal spectral emissivity at 807 and 940 nm and heat capacity at constant pressure of Pd–Fe melts were measured under electromagnetic levitation with a static magnetic field. The samples were made of Fe of mass purity 99.9985%. The present emissivity of Fe melts was relatively low compared with previously reported data using Fe with purity lower than 99.95% mass purity. The spectral emission of the Fe melts was analyzed using their normal spectral emissivity obtained from the Drude model. The excess heat capacity of Pd–Fe melts was evaluated from the measured heat capacity of Pd–Fe melts. Applying the Lupis–Elliot rule, we concluded from the obtained excess heat capacity that the enthalpy of mixing and excess entropy of the Pd–Fe melts should be negative. The composition dependence of the enthalpy of mixing, excess entropy, and excess Gibbs energy of Pd–Fe melts were evaluated using data obtained in this study and the literature.

Keywords: Electromagnetic levitation, Pd–Fe melts, Normal spectral emissivity, Heat capacity at constant pressure, Excess heat capacity, Enthalpy of mixing

*Corresponding authors: Manabu Watanabe (watanabe.m.cb@m.titech.ac.jp), and Hiroyuki Fukuyama (hiroyuki.fukuyama.b6@tohoku.ac.jp)

1 INTRODUCTION

Over the past 80 years, the correlation between excess volume (V^E) and thermodynamic functions of binary alloy melts has been studied [1–15]. In 1937, Scatchard [1] reported that the change in volume that occurs in mixing binary alloy melts had a significant correlation with both entropy and enthalpy of mixing ($\Delta_{mix}H$), but only a small correlation with Gibbs energy of mixing. Kleppa [2, 3] proposed expressions relating V^E and various thermodynamic functions involving coefficients of thermal expansion and assuming isothermal compressibility. Predel and Eman [4] showed that binary liquid alloy systems having large V^E values did not obey Scatchard's model, and Crawley [5] also reported a lack of correlation between the signs of V^E and $\Delta_{mix}H$ or the excess entropy (S^E). However, Marcus [6] presented a good correlation between the signs of V^E and S^E data obtained for liquid binary alloys having solid solutions or eutectic reactions in their phase diagrams. Kubaschewski and Alcock [7] also demonstrated a correlation between V^E and S^E, and between V^E and $\Delta_{mix}H$ for binary alloy systems. In 1988, Iida and Guthrie [8] summarized the correlations between V^E and $\Delta_{mix}H$ and stated that $\Delta_{mix}H$ and V^E are negative for compound-forming systems and positive for miscibility gap systems. This occurs because the interatomic distances established through the attractive interactions between atoms of different species decreases. Repulsive interactions have the opposite effect.

In contrast, Amore and colleagues [9] predicted systems having V^E and $\Delta_{mix}H$ with opposite signs using molecular dynamics simulations in conjunction with the Lennard-Jones interaction potential. Our group found that some binary systems exhibiting order–disorder transitions in the solid state show $V^E \geq 0$ and $\Delta_{mix}H \leq 0$ in the liquid state [10–13]. We proposed the liquid model based on the correlation between V^E and excess Gibbs energy (G^E) instead of $\Delta_{mix}H$ because G^E reflects both interatomic interactions ($\Delta_{mix}H$) and atomic arrangements (associated with entropy S^E) in the melt, and the minimization of G^E was determined to produce a thermodynamically stable atomic arrangement in the alloy. Brillo and colleagues [14] proposed a different liquid model based on the thermodynamic relationships between V^E and G^E of binary melts, using isothermal compressibility data determined from ultrasound velocity results. They concluded by adding that further assessment of the correlation between V^E and G^E in binary melts having order–disorder transitions would be interesting. However, for Pd–Fe melts, this correlation has been difficult to pin down because $\Delta_{mix}H$ and G^E have been reported as both positive and negative [15–22].

In this study, to determine whether the $\Delta_{mix}H$ and G^E values of Pd–Fe melts are positive or negative, the molar heat capacity at constant pressure (C_P) of these melts was measured through laser modulation calorimetry using a high-temperature thermophysical property measurement system (PROSPECT),

developed by various members of our group [10–13, 25–34]. Regarding the PROSPECT apparatus, a static magnetic field is applied to a droplet undergoing electromagnetic levitation, which significantly reduces the translational motion of the droplet and the surface oscillations of the droplet, allowing for highly accurate thermophysical properties measurements. For the Pd–Fe melts, $\Delta_{mix}H$, S^E, and G^E were calculated from excess heat capacity (C_P^E); the sign of $\Delta_{mix}H$ is evaluated based on the Lupis–Elliot rule [23, 24]. The normal spectral emissivity (ε) of the Pd–Fe melts was also measured to obtain the laser absorptivity required for the laser modulation calorimetry. The ε of liquid iron was analyzed from mass purity effects and a comparison with the Drude model.

2 MATERIALS AND MEASUREMENT METHODS

2.1 Sample preparation

The chemical compositions of the samples of Fe (99.9985% mass purity) [35] and Pd (99.95% mass purity, Rare Metallic Co., Ltd, Tokyo, Japan) are listed in Table 1. Chemical analysis of Fe and Pd was performed using glow discharge mass spectrometry. Purification involving anion exchange separation and plasma arc melting was conducted to prepare high purity Fe [35]. Samples with mole fractions of Fe (x_{Fe}) = 1, 0.8, 0.6, 0.4, and 0.2 were prepared by the arc melting method using the Fe and Pd listed in Table 1.

2.2 Measurement of thermophysical properties using PROSPECT

The experimental apparatus and detailed procedures were previously reported [27, 28, 34], therefore, only a brief account is presented here. The experimental equipment PROSPECT (Figure 1) includes a chamber evacuated to 10^{-3} Pa using a turbo-molecular pump. After evacuation, the chamber is filled using Ar-5 vol% H_2 gas up to normal pressure. The Pd–Fe samples are levitated and melted by generating an alternating current of 380 to 470 A in the levitation coil. A flow of He gas maintains the temperature of the sample.

TABLE 1
Chemical compositions of starting materials.

Chemical composition of the iron at initial sample (mass %) [28]										
Ca	**Al**	**Mg**	**Mn**	**Si**	**P**	**Co**	**Cr**	**Ni**	**Cu**	**Fe**
0.0000018	0.000011	0.0000003	0.0000022	0.000011	0.000015	0.00017	0.0000037	0.000013	0.0012	99.9985

Chemical composition of the palladium at initial sample (mass %)										
Mg	**Ca**	**Cr**	**Fe**	**Cu**	**Ru**	**Rh**	**Ag**	**Pt**	**Au**	**Pd**
0.00048	0.00017	0.00012	0.0012	0.00293	0.00047	0.00093	0.00014	0.01262	0.00048	99.95

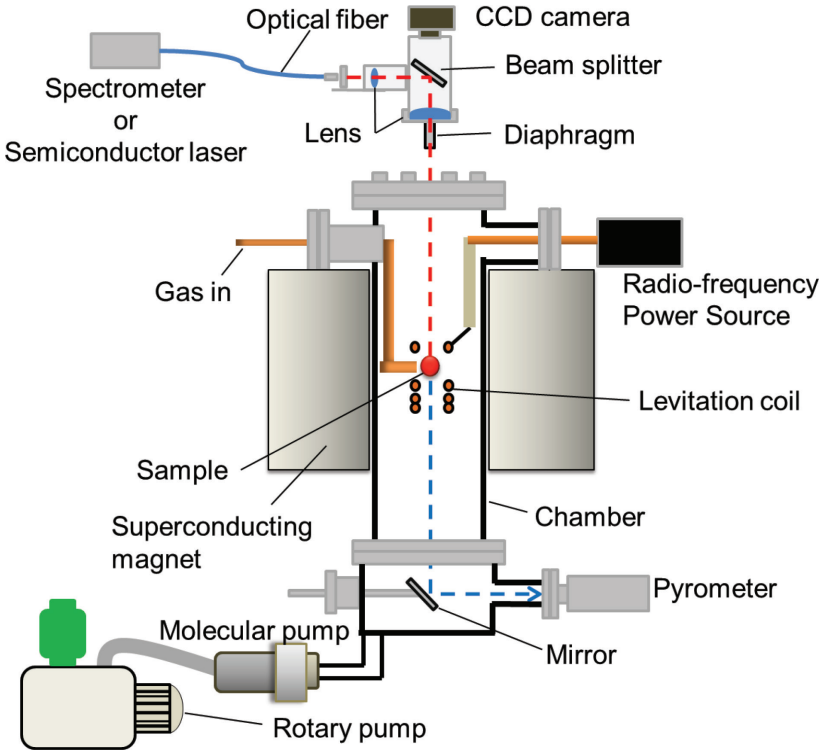

FIGURE **1**
Schematic of electromagnetic levitation (PROSPECT).

A single-color pyrometer (detection wavelength range: 1.45 – 1.8 μm, IGA140/MB25, LumaSense Technologies, Frankfurt, Germany), calibrated using the melting point or liquidus temperatures of Pd–Fe melts [36], is employed to measure the temperature at the bottom of the levitated sample. Temperatures other than the liquidus temperature were determined by assuming that at the pyrometer detection wavelength the normal spectral emissivity of the liquids does not depend on temperature.

2.2.1 Normal spectral emissivity measurement
The normal spectral emissivity (ε) is expressed as

$$\varepsilon(\lambda,T) = \frac{R_s(\lambda,T)}{R_B(\lambda,T)}, \tag{1}$$

where $R_s(\lambda,T)$ and $R_B(\lambda,T)$ denote the normal spectral emissive power emitted from the sample and from a blackbody, respectively, the latter $R_B(\lambda,T)$ being calculated from Planck's law. The normal spectral emissive power from the top of the sample droplet was measured using a multichannel

spectrometer (USB2000, Ocean Optics Inc., FL, USA), calibrated using a quasi-blackbody [26] made of graphite with a cavity at the center of the top face. The cavity is surrounded by a metal bath of Cu of Ni. The melting point of Cu (1357.8 K) and the eutectic temperature of the Ni–C system (1599.7 K) are then used for the calibration of the spectrometer. Using the quasi-blackbody, the relationship between $R_s(\lambda,T)$ and the output count of the spectrometer ($X(\lambda,T)$) was evaluated, being expressible as:

$$R_s\left(\lambda,T\right)=C\left(\lambda\right)\cdot X\left(\lambda,T\right), \tag{2}$$

where $C(\lambda)$ is a coefficient. The sample was levitated electromagnetically in a static magnetic field of 4 T.

2.2.2 Heat capacity measurement

The molar heat capacity at C_P was measured through laser modulation calorimetry [31, 34]. The levitated sample melt was heated from the top by modulated laser beam of power expressed as $P_0(1 + \cos \omega t)$ with an angular frequency (ω). The temperature response was observed at the bottom of the sample using a pyrometer. The temperature difference (ΔT_{ac}) and phase shift between the laser intensity and temperature response ($\Delta\phi$) are expressible as:

$$C_P=\frac{\alpha P_0 M}{\omega m\Delta T_{\mathrm{ac}}}\left(1+\frac{1}{\omega^2{\tau_{\mathrm{r}}}^2}+\omega^2{\tau_{\mathrm{c}}}^2\right)^{-\frac{1}{2}}, \tag{3}$$

$$\Delta\phi=\arccos\left\{\frac{\tau_{\mathrm{c}}}{\omega}\left(\frac{1}{\tau_{\mathrm{c}}\tau_{\mathrm{r}}}-\omega^2\right)f\right\}, \tag{4}$$

$$f=\left(1+\frac{1}{\omega^2{\tau_{\mathrm{r}}}^2}+\omega^2{\tau_{\mathrm{c}}}^2\right)^{-\frac{1}{2}}, \tag{5}$$

where α denotes the laser absorptivity of the sample, M the molar mass of the sample, m the sample mass, and f the correction function; τ_r and τ_c denote the external and the internal thermal relaxation times, respectively. According to Kirchhoff's law, α is equal to ε for an opaque sample. Quasi-adiabatic conditions, i.e., $\omega^2\tau_r^2>>1>>\omega^2\tau_c^2$, which implies $f \approx 1$, is achieved through an appropriate choice of modulation frequency and static magnetic field. Thermal relaxation times are determined through curve fitting Equation (4) to a measured relation between $\Delta\phi$ and the modulation frequency. To satisfy the adiabatic condition, a magnetic field intensity between 2.5 and 4 T was applied to reduce the internal relaxation time present in a residing convection flow in the droplet. In this study, f ranged from 0.97 to 0.99. The value of C_P was determined from τ_c, τ_r, and ΔT_{ac} using Equation (3).

3 RESULTS

3.1 Normal spectral emissivity

Figure 2 and Table 2 present the wavelength dependence of the normal spectral emissivity (ε) of Fe melt; the literature values [34, 37–48] are also given. The error bars in Fig. 2 represent the expanded uncertainties (95.45% confidence), which are described in Sec. 4.1.1. Comparison between the present work and the value obtained from the Drude model are discussed in Sec. 4.2. For the present work, ε of the Fe melt was measured over a wavelength range between 807 and 1000 nm. ε decreased monotonically with increasing wavelength in Fig. 2. The absorptivity of the laser used in the laser modulation calorimetry in this study is ε of Fe at 940 nm. ε of Fe at 807 nm was included for comparison with previously reported data. Therefore, ε of Fe at 807 and 940 was reported in the measured continuous wavelength range in this study. In addition, ε of Fe at 900 and 1000 was also reported as shown in Table 2.

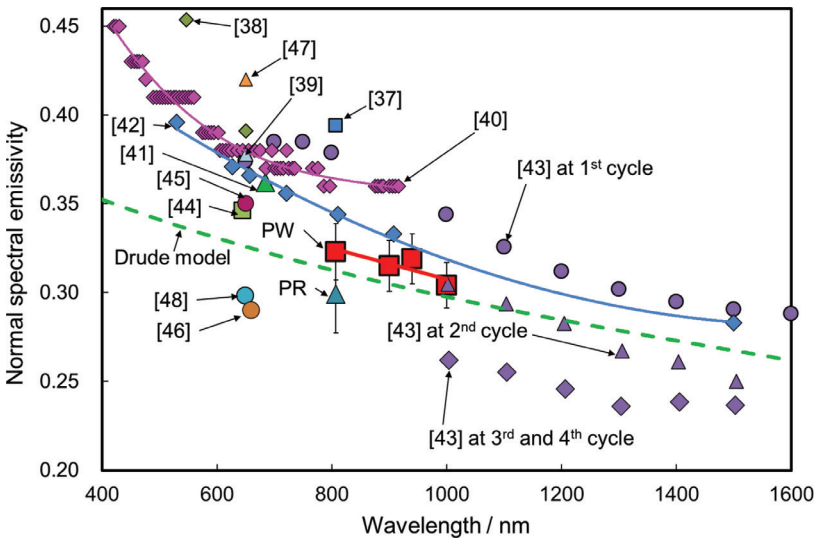

FIGURE 2
Wavelength dependence of the normal spectral emissivity of Fe melts at melting point. PW: Present work (EML with spectrometer, 99.9985% mass purity), PR: Previous work [34] (EML with spectrometer, 99.99% mass purity), [37]: Kobatake et al. (EML with spectrometer, 99.5% mass purity), [38]: Schaefers et al. (EML with pyrometer, no sample purity information), [39]: Treverton and Margrave (EML with pyrometer, 99.9% mass purity), [40]: Krishnan et al. (EML with ellipsometer, 99.95% mass purity), [41]: Wilthan et al. (Pulse heating technique with polarimeter, 99.5% mass purity), [42]: Kaschnitz et al. (Pulse heating technique with pyrometer, 99.99% mass purity), [43]: Watanabe et al. (Cold crucible with spectrometer, 99.99% mass purity), [44]: Ratanapupech and Bautista (Crucible with pyrometer, 99.99% mass purity), [45]: Mori et al. (MgO crucible with pyrometer, no sample purity information), [46]: Bidwell (Graphite crucible with pyrometer, no sample purity information), [47]: Dastur and Gokcen (Beryllia crucible with pyrometer, no sample purity information), [48]: Lange and Schenck (Crucible with pyrometer, no sample purity information).

TABLE 2
Normal spectral emissivity of Fe melts at melting point.

Reference	Method	Sample purity (mass %)	Wavelength, λ/ nm	Normal spectral emissivity, ε
Present work	EML with spectrometer	99.9985	807	0.324
			900	0.315
			940	0.319
			1000	0.304
Previous work [34]	EML with spectrometer	99.99	807	0.30
Kobatake et al. [37]	EML with spectrometer	99.5	807	0.394
Schaefers et al. [38]	EML with pyrometer	No information	547 650	0.424 0.365
Treverton and Margrave [39]	EML with Pyrometer	99.9	650	0.378
Krishnan et al. [40]	EML with ellipsometer	99.95	420 to 916	$-7{\cdot}10^{-10}{\cdot}\lambda^3+2{\cdot}10^{-6}{\cdot}\lambda^2$ $-1.6{\cdot}10^{-3}{\cdot}\lambda+0.862$
Wilthan et al. [41]	Pulse heating technique with polarimeter	99.5	684.5	0.362
Kaschnitz et al. [42]	Pulse heating technique with pyrometer	99.99	530 627 657 721 811 908 1500	0.396 0.371 0.366 0.356 0.344 0.333 0.283
Watanabe et al. (at 1st cycle) [43]	Cold crucible with spectrometer	99.99	650 to 800	$-3.045+(1.2973{\cdot}10^{-2}){\cdot}\lambda$ $-1.62{\cdot}10^{-5}{\cdot}\lambda^2$ $+(6.6667){\cdot}10^{-9}{\cdot}\lambda^3$
			1000 to 1900	$0.90125-1.0098{\cdot}10^{-3}{\cdot}\lambda$ $+5.5366{\cdot}10^{-7}{\cdot}\lambda^2$ $-1.0128{\cdot}10^{-10}{\cdot}\lambda^3$
Ratanapupech and Bautista [44]	Crucible with pyrometer	99.99	645	0.346
Mori et al. [45]	MgO crucible with pyrometer	No information	650	0.35
Bidwell [46]	Graphite crucible with pyrometer	No information	660	0.29
Dastur and Gokcen [47]	Beryllia crucible with pyrometer	No information	650	0.42
Lange and Schenck [48]	Crucible with pyrometer	No information	650	0.298

In our previous work [34], ε of a Fe melt (99.99 mass% purity) was measured at 807 nm using the same apparatus. Kashnitz and colleagues [42] measured the ε of Fe melt of 99.99 mass% in purity in a wavelength region between 530 and 1500 nm employing the pulse heating technique. Our present data agreed with our previous [34] data and that of [42] within experimental uncertainties. Watanabe and colleagues [43] measured ε of a Fe melt of 99.99% mass purity four times consecutively using a cold crucible in which the sample was set on a MgO substrate; they found that ε decreased with each additional measurement cycle, the reason being that a MgO film covered the molten Fe surface. The ε of MgO in a solid state was reported as 0.227 at 1000 nm at 1600 K [51], which is smaller than that of Fe melt. Kobatake and colleagues [37] measured ε of Fe melts of 99.5% mass purity at 807 nm using PROSPECT, whereas Krishnan and colleagues [40] measured ε of a Fe melt of 99.95% mass purity under electromagnetic levitation through ellipsometry. For both groups, ε of the Fe melts measured were larger than those measured in the present work. Morohoshi and colleagues [49, 50] proposed that the Fe samples with relatively low mass purity might be covered by oxide impurities such as Al_2O_3 film under an atmosphere with oxygen activity over 10^{-11}. The ε values of Al_2O_3 at 640 nm at 1773 K and at 1000 nm at 1858 K were reported as 0.388 and 0.500 [52], respectively. An Al_2O_3 film may have caused the large emissivity of Fe melt in the experiments performed by the Kobatake and Krishnan groups.

Figure 3 and Table 3 present the temperature dependence of ε for Pd–Fe melts at 807 and 940 nm. The ε of Pd melt was measured previously by the present authors using the same method [27]. Again, the error bars represent the expanded uncertainty, which is discussed in Section 4.1.1. For all Pd–Fe melts, no temperature dependence in ε is evident, and therefore, ε for each Pd–Fe melt was determined as an average value. Figure 4 plots the composition dependence of ε of each Pd–Fe melt at 807 and 940 nm and assumes the temperature dependence of ε of Pd–Fe melts between 1585 and 1853 K is negligible. A local maximum exists at $x_{Fe} = 0.6$ (Fig. 4).

3.2 Molar heat capacity at constant pressure

Figure 5(a) plots the temperature modulation on the top of a sample irradiated by the laser beam and the temperature response measured at the bottom of the sample during laser modulation calorimetry. The sample is a Pd–Fe melt of mole fraction $x_{Fe} = 0.4$ at laser modulation frequency of 0.04 Hz under a static magnetic field of 3.2 T. Figure 5(b) shows phase shift ($\Delta\phi$) and $\omega\Delta T_{ac}$ as a function of laser modulation frequency at 1685 K. The value of $\omega\Delta T_{ac}$ is 6.34 K·rad·s^{-1} at a laser modulation frequency of 0.2 Hz and satisfies the adiabatic condition corresponding to $\Delta\phi = 90°$. By curve fitting the relationship between modulation frequency and phase shift using Equation (4), τ_r, τ_c, and f were evaluated, respectively as 0.13 s, 5.97 s, and 0.98.

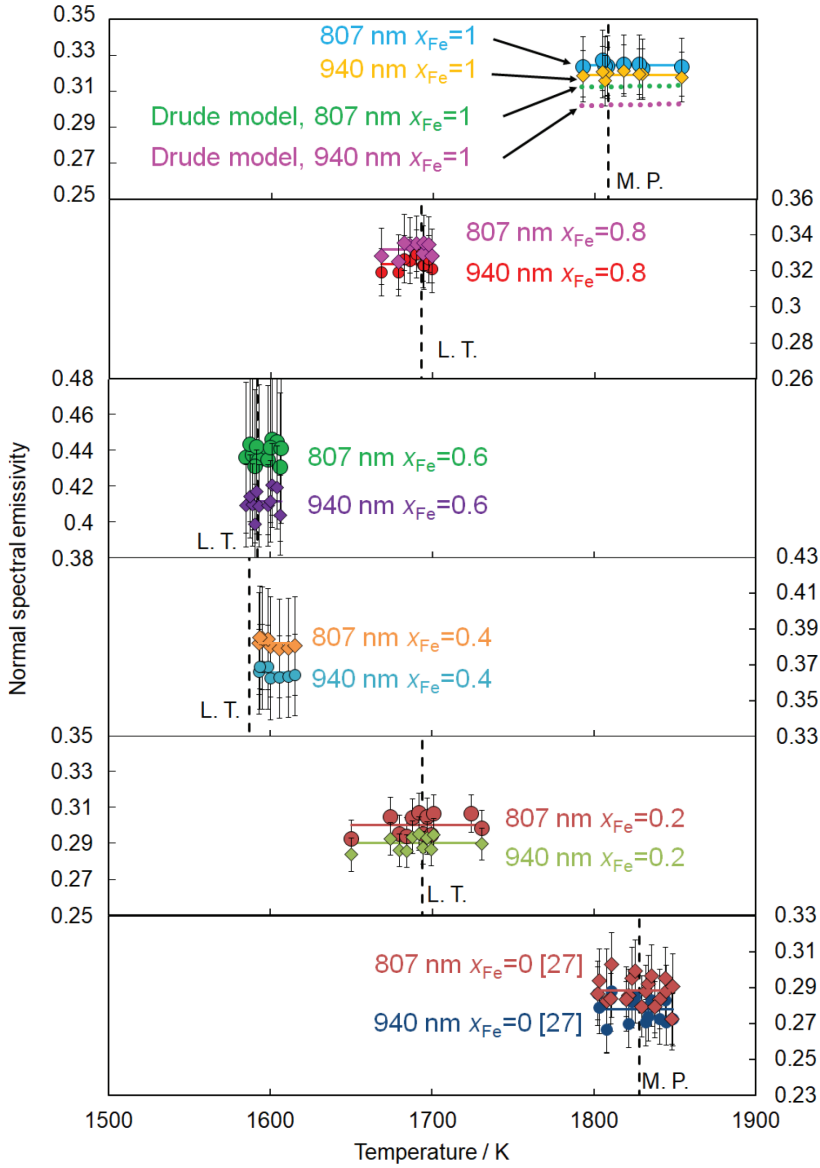

FIGURE 3
Temperature dependence of the normal spectral emissivity of Pd–Fe melts. The black dashed line indicates the melting point or liquidus temperature. The error bars represent the expanded uncertainty (95.45% confidence).

C_P of the Pd–Fe melts were obtained from Equation (3) using $\omega\Delta T_{ac}$ and its temperature dependence measured in the present work is presented in Fig. 6 and Table 4. The present authors measured C_P of Fe and Pd melts

TABLE 3
Emissivity of the Pd–Fe melts at 807 and 940 nm

Reference	x_{Fe}	Temperature / K	Wavelength, λ / nm	Normal spectral emissivity, ε	Average of expanded uncertainty (95.45 % confidence)
[27]	0	1802–1849	807	0.288	0.017
			940	0.278	0.014
Present work	0.2	1650–1731	807	0.300	0.010
			940	0.290	0.009
Present work	0.4	1593–1615	807	0.382	0.028
			940	0.366	0.023
Present work	0.6	1585–1607	807	0.438	0.042
			940	0.411	0.023
Present work	0.8	1668–1699	807	0.332	0.015
			940	0.324	0.013
Present work	1	1792–1853	807	0.324	0.016
			940	0.319	0.014

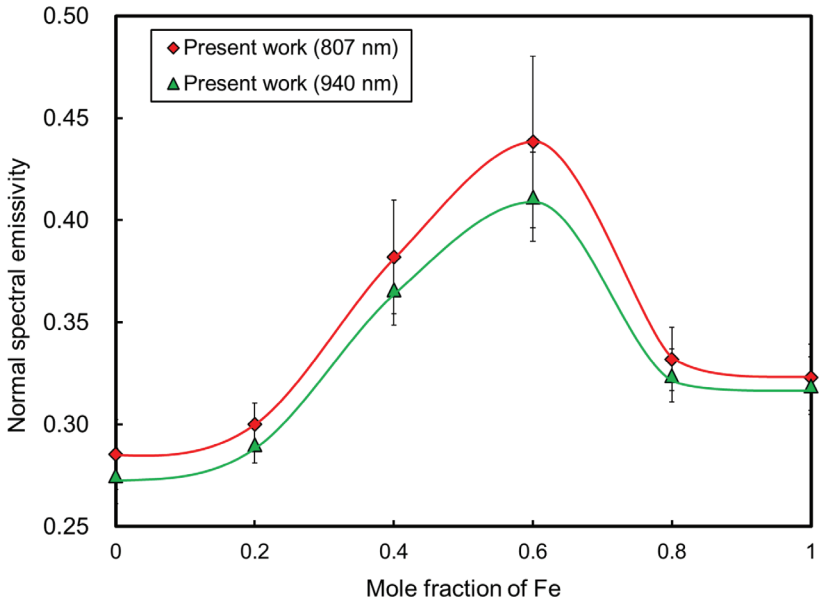

FIGURE 4
Composition dependence of the emissivity of Pd–Fe melts between 1585 and 1853 K at 807 and 940 nm. The error bars represent the expanded uncertainty (95.45% confidence).

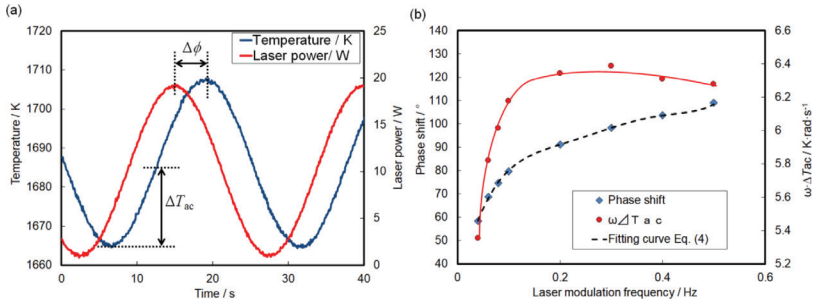

FIGURE **5**
(a) Laser power (right-hand ordinate) and temperature response (left-hand ordinate) of Pd–Fe melts of $x_{Fe} = 0.4$ during laser modulation calorimetry at 0.04 Hz under 3.2 T, (b) Phase shift (right-hand ordinate) and $\omega \cdot \Delta T$ac (left-hand ordinate) as functions of the laser modulation frequency of Pd–Fe melts of $x_{Fe} = 0.4$ at 1685 K under 3.2 T.

previously employing the same method [27, 32]. The comparison between the heat capacity measured by the authors and reported by other researchers for Fe and Pd was already conducted in the previous paper [27, 34]. Within experimental uncertainty, C_P for the Pd–Fe melts shows a negligible temperature dependence. The uncertainty is discussed in Sec. 4.1.2. Wilde and colleagues [53–55] measured C_P of Pd–Fe melts in an undercooling temperature region at $x_{Fe} = 0.5$ and 0.8 using differential scanning calorimetry (DSC). In their study, the sample was embedded on a Duran glass to prevent nucleation in the sample melts. With increasing temperature, C_P of Pd–Fe at $x_{Fe} = 0.5$ and 0.8 measured by Wilde's group decreased. Figure 7(a) shows the composition dependence of C_P for each Pd–Fe melt assuming that C_P has no temperature dependence between 1412 K and 1996 K.

The present work is in good agreement with the data for $x_{Fe} = 0.8$ from Wilde's group [53, 54]; however, their data at $x_{Fe} = 0.5$ did not agree well with the present work. We note that Duran glass consists of SiO_2, B_2O_3, Na_2O, K_2O, and Al_2O_3 and is in a liquid state at 880 K [56, 57]. Boron and oxygen within the Duran glass have high chemical activity, and therefore, Pd–Fe melts may have been contaminated by these elements in the experiment of Wilde's group.

4 DISCUSSION

4.1 Uncertainty analysis

In this study, the measurement uncertainty was evaluated based on the Guide to the Expression of Uncertainty in Measurement (GUM) [58].

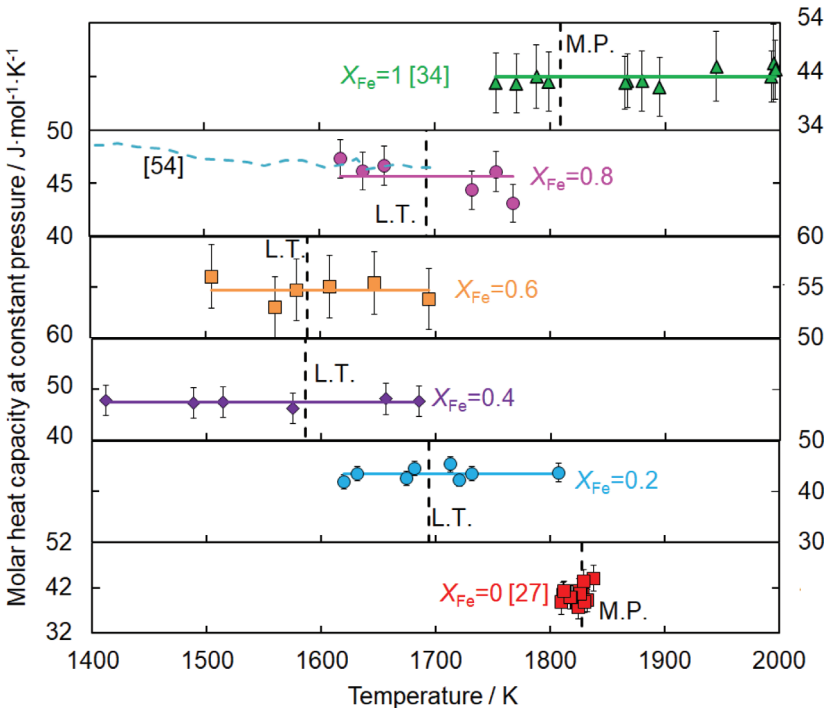

FIGURE 6
Temperature dependence of the molar heat capacity at constant pressure of Pd–Fe melts. The error bars show the expanded uncertainty (95.45% confidence). The black dashed lines indicate melting point or liquidus temperature. [54]: Wilde et al. (DSC).

TABLE 4
Heat capacity at constant pressure of Pd–Fe melt.

Reference	**Method**	**Composition of Fe, x_{Fe}**	**Temperature range, T / K**	**Heat capacity at constant pressure, Cp / J·mol^{-1}·K^{-1}**
[27]	Laser modulation calorimetry	0	1810–1838	40.5
Present work		0.2	1620–1807	43.5
Present work		0.4	1412–1685	47.5
Present work		0.6	1506–1695	54.7
Present work		0.8	1618–1768	45.6
[34]		1	1753–1996	44.0
Wilde et al. [53–55]	DSC	0.5	1373–1620	44.1–44.8
		0.8	1372–1698	46.3–48.1

4.1.1 Uncertainty analysis of normal spectral emissivity measurements
The uncertainty of the normal spectral emissivity is expressed as:

$$u^2(\varepsilon) = \left(\frac{\partial \varepsilon}{\partial C}\right)^2 u^2(C) + \left(\frac{\partial \varepsilon}{\partial T}\right)^2 u^2(T_{\text{Pyro}}) + \left(\frac{\partial \varepsilon}{\partial T}\right)^2 u^2(T_{\text{Cal}}), \tag{6}$$

where $u(\varepsilon)$ denotes the combined standard uncertainty of the normal spectral emissivity, $u(C)$ the uncertainty of calibration coefficient C in Eq. (2) [26], $u(T_{\text{Pyro}})$ the accuracy of the pyrometer reported by the manufacturer, and $u(T_{\text{Cal}})$ the uncertainty of the pyrometer calibration using the temperature profile at liquidus temperature. $u(T_{\text{Pyro}})$ was reported by the manufacturer of the pyrometer as 0.3% of the measured value plus 1°C up to 1500°C and 0.5% of the measured value above 1500°C. As an example, the uncertainty evaluation of the emissivity for Pd–Fe melts of $x_{\text{Fe}} = 0.6$ at 1587 K is presented in Table 5. The dominant contribution in the uncertainty was $u(C)$ and the expanded uncertainty ($U = 2u(\varepsilon)$) was 0.042, which corresponds to 9.9% of the emissivity. The value of U for each Pd–Fe melt is presented in Table 3.

4.1.2 Uncertainty analysis of heat capacity
The uncertainty of the heat capacity is given as:

$$u^2(C_P) = \left(\frac{\partial C_P}{\partial \varepsilon}\right)^2 u^2(\varepsilon) + \left(\frac{\partial C_P}{\partial \Delta T_{ac}}\right)^2 u^2(\Delta T_{\text{ac}}) + \left(\frac{\partial C_P}{\partial m}\right)^2 u^2(m) + \left(\frac{\partial C_P}{\partial P_0}\right)^2 u^2(P_0), \tag{7}$$

TABLE 5
Uncertainty evaluation in normal spectral emissivity measurements of 807 nm of Pd–Fe melt of $x_{\text{Fe}} = 0.6$ at 1587 K.

Component	Standard uncertainty	Sensitivity coefficient	Contribution
Uncertainty of coefficient: $u(C)$	5.05×10^{-3} W·m^{-2}·μm^{-1}	$\frac{\partial \varepsilon}{\partial C} =$ 3.06 W^{-1}·m^2·μm	1.55×10^{-2}
Accuracy of pyrometer: $u(T_{\text{Pyro}})$	2.39 K	$\frac{\partial \varepsilon}{\partial T} =$ -3.21×10^{-3} K^{-1}	-7.45×10^{-3}
Uncertainty of pyrometer calibration at liquids temperature: $u(T_{\text{cal}})$	3.90 K	$\frac{\partial \varepsilon}{\partial T} =$ -3.13×10^{-3} K^{-1}	-1.22×10^{-3}
Combined standard uncertainty $u(\varepsilon)$			0.021
Expanded uncertainty $U = 2u(\varepsilon)$ (95.45 % confidence)			0.042

$\varepsilon = 0.442$ for Pd–Fe melt of $x_{\text{Fe}} = 0.6$ at 1587 K

TABLE 6
Uncertainty evaluation in heat capacity measurements for Pd–Fe melt of $x_{Fe} = 0.4$ at 1575 K.

Component	Standard uncertainty	Sensitivity coefficient	Contribution
Uncertainty of normal spectral emissivity: $u(\varepsilon)$	2.3×10^{-2}	$\frac{\partial C_P}{\partial \varepsilon} =$ 126 J·mol^{-1}·K^{-1}	1.5 J·mol^{-1}·K^{-1}
Uncertainty of temperature amplitude: $u(\Delta T_{ac})$	3.0×10^{-2} K	$\frac{\partial C_P}{\partial \Delta T_{ac}} =$ −8.4 J·mol^{-1}·K^{-2}	-2.6×10^{-1} J·mol^{-1}·K^{-1}
Uncertainty of mass loss due to evaporation: $u(m)$	1.6×10^{-7} kg	$\frac{\partial C_P}{\partial m} =$ 5.0×10^4 J·kg^{-1}·mol^{-1}·K^{-1}	7.8×10^{-3} J·mol^{-1}·K^{-1}
Uncertainty of accuracy of laser power $u(P_0)$	3.0×10^{-3} W	$\frac{\partial C_P}{\partial P_0} =$ 5.1 s·mol^{-1}·K^{-1}	1.5×10^{-2} J·mol^{-1}·K^{-1}
Combined standard uncertainty of heat capacity			1.5 J·mol^{-1}·K^{-1}
Expanded uncertainty $U = 2u(C_P)$ (95.45 % confidence)			3.0 J·mol^{-1}·K^{-1}

$Cp = 46.2$ J·mol^{-1}·K^{-1} for Pd–Fe melt of $x_{Fe} = 0.4$ at 1575 K

where $u(C_P)$ denotes the combined standard uncertainty in the molar heat capacity; $u(\varepsilon)$, $u(\Delta T_{ac})$, $u(m)$, and $u(P_0)$ denote respectively the uncertainties in the normal spectral emissivity, temperature amplitude, sample mass through vaporization of the sample, and accuracy of the laser beam power. As an example, the uncertainty evaluation of the heat capacity measurement in the Pd–Fe melt of $x_{Fe} = 0.4$ at 1575 K is presented in Table 6. The dominant contribution to the uncertainty is $u(\varepsilon)$ and the expanded uncertainty ($U = 2u(C_P)$) is 3.0 J·mol^{-1}·K^{-1}, which corresponds to 6.4% of the heat capacity. In this study, U for all measurements of the Pd–Fe melts at $x_{Fe} = 0.2$, 0.4, 0.6, and 0.8 range from 3.2% to 4.2%, 6.3% to 6.4%, 5.6% to 5.7%, and 3.9% to 4.1%, respectively.

4.2 Normal spectral emissivity of Fe melt calculated based on the Drude model

In our previous paper [34], ε of the Fe melt was calculated based on the Drude model. The wavelength dependence of the calculated ε at the melting point (see Fig. 2 and Table 7) decreases with increasing wavelength. The temperature dependence of the calculated ε at 807 and 940 nm (Fig. 3 and Table 7) displays a slight increase with increasing temperature. The experimentally obtained data in this study over a wavelength range between 807 and 1000 nm were slightly larger than calculated values. Hayashi and colleagues [59]

TABLE 7
Values used to calculate normal spectral emissivity of Fe melts by the Drude model at melting point.

Properties	Values of Fe melts
Temperature T / K	1792 to 1854
Density ρ / kg·m^{-1} [10]	$(-0.822)\cdot(T-1808)+7043$
Electrical resistivity ρ_{el} / Ω·m [60]	$1.78\times10^{-10}\cdot T+1.18\times10^{-6}$
Number of free electrons per atom [61]	1.21
Number of free electrons per unit volume / m^{-3}	$-1.02\times10^{25}\cdot T+1.05\times10^{29}$
Plasma frequency / rad·s^{-1}	$-1.00\times10^{12}\cdot T+1.85\times10^{16}$
Relaxation time of free electrons / s	$3.84\times10^{-24}\cdot T^2+1.44\times10^{-20}\cdot T+2.85\times10^{-16}$
Electron mass / kg	9.11×10^{-31}
Permittivity of the vacuum / F·m^{-1}	8.85×10^{-12}
Charge of the electron / C	1.60×10^{-19}
Emissivity at 400 nm evaluated by Drude model	$-2.02\times10^{-9}\cdot T^2+2.57\times10^{-5}\cdot T+0.313$
Emissivity at 600 nm evaluated by Drude model	$-1.79\times10^{-9}\cdot T^2+2.32\times10^{-5}\cdot T+0.294$
Emissivity at 807 nm evaluated by Drude model	$-1.53\times10^{-9}\cdot T^2+2.13\times10^{-5}\cdot T+0.279$
Emissivity at 940 nm evaluated by Drude model	$-1.39\times10^{-9}\cdot T^2+2.04\times10^{-5}\cdot T+0.270$
Emissivity at 1000 nm evaluated by Drude model	$-1.34\times10^{-9}\cdot T^2+1.99\times10^{-5}\cdot T+0.266$
Emissivity at 1600 nm evaluated by Drude model	$-9.66\times10^{-10}\cdot T^2+1.70\times10^{-5}\cdot T+0.235$

described two mechanisms for spectral emissions from metals. They involve interband and intraband transitions of electrons. In the Drude model, the former are not considered. Nevertheless, from a comparison between the experimentally obtained and calculated ε, the contribution of the interband transitions is considered to be small.

4.3 Excess heat capacity and excess thermodynamic functions

Using the molar heat capacity at a constant pressure of an ideal solution (C_P^{ideal}), the excess molar heat capacity C_P^{E} is

$$C_P^{\text{E}} = C_P - C_P^{\text{ideal}}, \tag{8}$$

$$= \frac{\partial \Delta_{mix} H}{\partial T}, \tag{9}$$

$$= T\left(\frac{\partial S^{\text{E}}}{\partial T}\right), \tag{10}$$

$$C_P^{\text{ideal}} = \sum_{i=0}^{N} x_i \cdot C_{P,i} \cdot \tag{11}$$

Here, $C_{P,i}$ denotes the molar heat capacity of component i. In Fig. 7(a), C_P^{ideal} of the Pd–Fe melts is represented by a black dashed line. Clearly, the present data exhibits a positive deviation from the ideal solution over the whole composition range. Therefore, C_P^{E} of the Pd–Fe melts is positive at all mole fractions [Fig. 7(b)].

Both G^{E} and $\Delta_{\text{mix}}H$ of Pd–Fe melts were reported by many researchers [15–22]; their composition dependence reported in Refs. [15–18] is negative; in contrast, that reported in Refs. [19–22] is slightly positive. Aukrast and colleagues [15] measured the activities of Fe in the Pd–Fe system from oxidation experiments at a temperature range between 1473 and 1733 K. Lindscheid and Lange [16] measured the activities of Fe and Pd in Pd–Fe melts at 1823 and 1873 K employing the Knudsen and torsion methods. The group of Tomiska [17] measured the activities of Fe and Pd melts at 1850 K using Knudsen cell mass spectrometry whereas Ghosh and colleagues [18] determined the activities of Fe and Pd in the Pd–Fe melts from calculations using the PARROT module of the Thermo-Calc software. Vatolin and colleagues also determined the activities of Fe and Pd in the Pd–Fe melts at 1873 K employing both the Knudsen effusion method [19] and the EMF method [20]. Similarly, Hultgren [22] reported the same activities based on the activity obtained from the Vatolin group data [19, 20], which was also used by Koirala and colleagues [21] in estimating $\Delta_{\text{mix}}H$ using the quasi-chemical approximation.

To determine whether the $\Delta_{\text{mix}}H$ and G^{E} values of the Pd–Fe melts are positive or negative the temperature dependence of $\Delta_{\text{mix}}H$ and S^{E} of the Pd–Fe melts was calculated using C_P^{E} and the sign of the $\Delta_{\text{mix}}H$ was evaluated from the C_P^{E} based on the Lupis–Elliot rule [23, 24]. In addition, the $\Delta_{\text{mix}}H$, S^{E}, and G^{E} of Pd–Fe melts were evaluated using the obtained temperature dependence of the

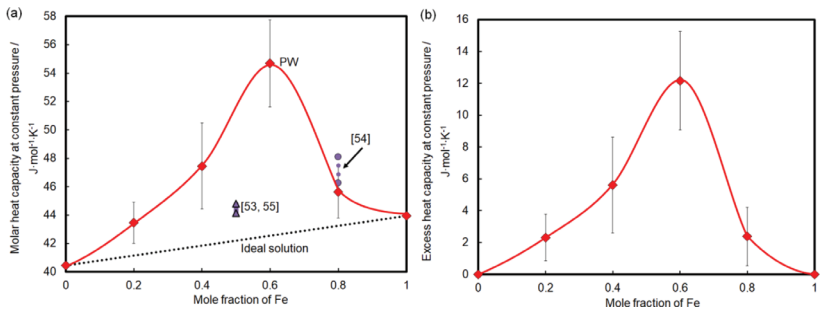

FIGURE 7
Composition dependence of (a) the molar heat capacity at constant pressure and (b) excess heat capacity of Pd–Fe melts between 1412 K and 1996 K. The error bars represent the expanded uncertainty (95.45% confidence). The black dashed line in (a) indicates the ideal solution. PW: Present work, [53–55]: Wilde et al. (DSC).

thermodynamic functions and literature data. The Lupis–Elliot rule describes solid, liquid, and gaseous solutions (and pure gases) as gradually approaching the state of an ideal solution (perfect gas) with increasing temperature at any pressure and composition. On that basis, Kaptay and colleagues surmised [24]

1. $\Delta_{mix}H$ and S^E have the same signs, and
2. $\Delta_{mix}H$ and $C_P{}^E$ have opposite signs.

From the positive sign of $C_P{}^E$ and the Lupis–Elliot rule, $\Delta_{mix}H$ of the Pd–Fe melts should be negative at all mole fractions.

Finally, the composition dependence of enthalpy of mixing $\Delta_{mix}H(T)$, excess $S^E(T)$, and excess $G^E(T)$ were evaluated using the obtained temperature dependence of the thermodynamic functions and literature data; they were calculated from:

$$\Delta_{mix}H(T) = \Delta_{mix}H(T_{Ref}) + \int_{T_{Ref}}^{T} C_P{}^E dT, \tag{12}$$

$$S^E(T) = S^E(T_{Ref}) + \int_{T_{Ref}}^{T} \frac{1}{T} C_P{}^E dT, \tag{13}$$

$$G^E(T) = \Delta_{mix}H(T) - TS^E(T), \tag{14}$$

$$= G^E(T_{Ref}) + \int_{T_{Ref}}^{T} C_P{}^E \left(1 - \frac{1}{T}\right) dT. \tag{15}$$

Here, $\Delta_{mix}H(T_{Ref})$, $S^E(T_{Ref})$, and $G^E(T_{Ref})$ are the corresponding quantities taken at reference temperature T_{Ref} , which, for this study, is $T_{Ref} = 1850$ K, and were reported in Ref. [17]. Figure 8 shows the composition dependence of (a) $\Delta_{mix}H$, (b) S^E, and (c) G^E. With increasing temperature, $\Delta_{mix}H$ and S^E approached the ideal solution model. G^E exhibits negative values over the whole mole fraction range. The temperature dependence of G^E is almost negligible at temperatures between 1750 and 2000 K.

On the basis of the Lupis–Elliot rule, all the excess thermodynamic functions including G^E should approach the ideal solution when temperatures are large. However, in drawing Fig. 8, C_P (and $C_P{}^E$) for each Pd–Fe melt was treated as a constant over the restricted temperature range, which is why G^E does not follow the Lupis–Elliot rule.

5 CONCLUSIONS

In this study, to determine whether the $\Delta_{mix}H$ and G^E values of Pd–Fe melts are positive or negative, the composition and temperature dependence of ε and C_P of Pd–Fe melts were measured. Both ε and C_P displayed no temperature dependence. Over a wavelength range between 807 and 1000 nm, ε of Fe melt

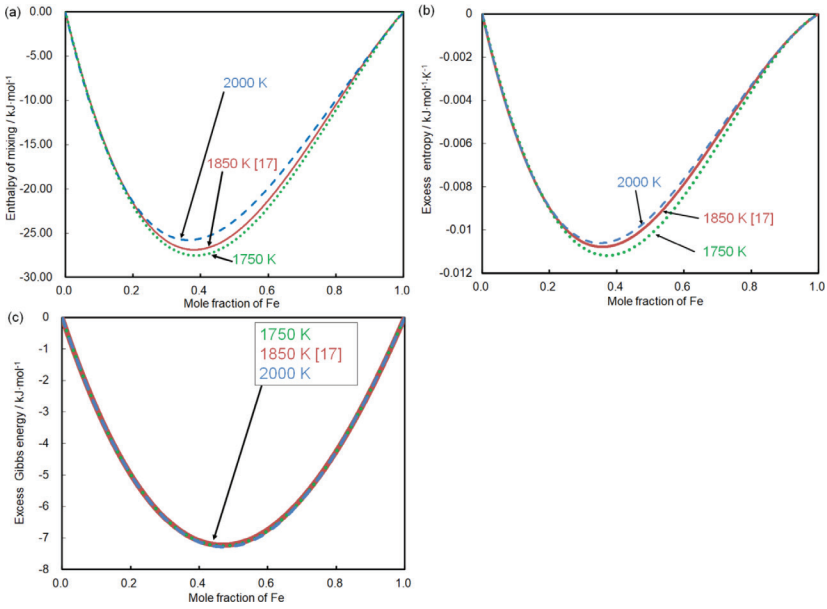

FIGURE 8
Composition dependence of (a) enthalpy of mixing, (b) excess entropy, and (c) excess Gibbs energy of Pd–Fe melts.

was larger than that for the Drude model because of contributions from interband transitions of electrons. Over the entire composition range, C_P^{E} of each Pd–Fe melt gave positive values, and therefore, we conclude that $\Delta_{\mathrm{mix}}H$ and S^{E} of Pd–Fe melts should have negative values based on the Lupis–Elliot rule. Using these C_P^{E} values, $\Delta_{\mathrm{mix}}H$, S^{E}, and G^{E} of the Pd–Fe melts were calculated; with increasing temperature, both $\Delta_{\mathrm{mix}}H$ and S^{E} approach the values obtained from the ideal solution model, being consistent with the Lupis–Elliot rule. We also observed that G^{E} takes negative values over the entire composition range.

Declaration of Competing Interest
The authors declare that they have no known competing financial interests or personal relationships that could have appeared to influence the work reported in this paper.

ACKNOWLEDGMENTS

This work was supported by the Japan Society for the Promotion of Science (JSPS) KAKENHI Grant 20K22464 and 21K14447. We thank Richard Haase, PhD, from Edanz (https://jp.edanz.com/ac) for editing a draft of this manuscript.

REFERENCES

[1] G. Scatchard, Change of volume on mixing and the equations for non-electrolyte mixtures, Trans. Faraday Soc., **33**(1937) 160–166. https://doi.org/10.1039/TF9373300160

[2] O. J. Kleppa, The volume change on mixing in liquid metallic solutions. I. Alloys of cadmium with indium, tin, thallium, lead and bismuth, J. Phy. Chem., **64**(1960) 1542–1546. https://doi.org/10.1021/j100839a049

[3] O. J. Kleppa, M. Kaplan, C. E. Thalmayer, The volume change on mixing in liquid metallic solutions II, J. Phys. Chem., **65**(1961)843–849. https://doi.org/10.1021/j100823a031

[4] B. Predel, A. Eman, überschubvolumina flüssiger Legierungen der Systeme Bi–Sn, Sn–Tl, Pb–Sn, Bi–Tl, Hg–In, Hg–Tl und Pb–Tl, Mater. Sci. Eng., **4**(1969) 287–296.

[5] A. F. Crawley, Densities of liquid metals and alloys, Int. Metall. Rev., **19**(1974) 32–48. https://doi.org/10.1179/imtlr.1974.19.1.32

[6] Y. Marcus, Introduction to liquid state chemistry, (1977), Ch.8, Wiley, London.

[7] O. Kubaschewski, C. B. Alcock, Metallurgical thermochemistry, 5th ed. Pergamon press, Oxford.

[8] T. Iida, R. I. L. Guthrie, The physical properties of Liquid Metals, Clarendon Press, Oxford, New York; (1988).

[9] S. Amore, J. Horbach, I. Egry, Is there a relation between excess volume and miscibility in binary liquid mixture? J. Chem. Phys., **134**(2011) 044515. https://doi.org/10.1063/1.3528217

[10] M. Watanabe, M. Adachi, H. Fukuyama, Densities of Fe-Ni melts and thermodynamic correlations, J. Mater. Sci., **51**(2016) 3303– 3310. https://doi.org/10.1007/s10853-015-9644-2

[11] M. Watanabe, M. Adachi, H. Fukuyama, Correlation between excess volume and thermodynamic functions of liquid Pd-X (X=Fe, Cu and Ni) binary systems, J. Chem. Thermodyn., **130**(2019) 9–16. https://doi.org/10.1016/j.jct.2018.09.037

[12] M. Watanabe, M. Adachi, H. Fukuyama, Correlation between excess volume and thermodynamic functions of liquid Pt-X (X=Fe, Co, Ni and Cu) binary systems, Fluid Phase Equilbr., **515**(2020)112596. https://doi.org/10.1016/j.fluid.2020.112596

[13] M. Watanabe, M. Adachi, H. Fukuyama, Densities of Au-X(X=Cu, Ni, and Pd) binary melts and thermodynamic correlations, J. Mol. Liq., **348**(2022)118050. https://doi.org/10.1016/j.molliq.2021.118050

[14] J. Brillo, M. Watanabe, H. Fukuyama, Relation between excess volume, excess free energy and isothermal compressibility in liquid alloys, J. Mol. Liq., **326**(2021) 114395. https://doi.org/10.1016/j.molliq.2020.114395

[15] E. Aukrust, A. Muan, Thermodynamic properties of Pd–Fe alloys in the temperature range 1200–1460°C, Acta Metallurgica, **10**(1962)555-560. https://doi.org/10.1016/0001-6160(62)90201-8

[16] H. Lindsheid, K. W. Lange, Aktivitätsbestimmungen im system Eisen-palladium mit einer kombinierten Knudsen-Torsions-methode, Arch. Eisen., **46**(1975) 423–425.

[17] J. Tomiska, P. Krajnik, A. Neckel, Ermittlung thermodynamischer Mischungseffekte von geschmolzenen Fe-Pd-Legierungen mit Hilfe der Knudsenzellen-Massenspektrometrie, Z. Metallkde, **80**(1989) 258–262.

[18] G. Ghosh, C. Kantner, G. B. Olson, Thermodynamic Modeling of the Pd-X(X=Ag, Co, Fe, Ni) Systems, J. Phase Equil., **20**(1999). https://doi.org/10.1361/105497199770335811

[19] N. A. Vatolin, A. I. Timofeev, E. L. Dubinin, ДАВЛЕНИЕ ПАРА ЖИДКИХ СПЛАОВ НА ОСНОВЕ ПАЛЛАДИЯ, Russ. J. Phys. Chem., **45**(1971) 2027–2029.

[20] N. A. Vatolin, A. I. Timofeev, O. A. Esin, E. L. Dubinin, ИЗУЧЕНИЕ АКТИВНОСТИ КОМПОНЕНТОВ В НЕКОТОРЫХ ЖИДКИХ МЕТАЛЛИЧЕСКИХ СПЛАВАХ НА ОСНОВЕ ПАЛЛАДИЯ МЕТОДОМ ЭЛЕКТРОДВИЖУЩИХ СИЛ, Russ. J. Phys. Chem. **45**(1971) 2021–2026.

[21] R. P. Koirala, J. Kumar, B. P. Singh, D. Adhikari, Bulk and Surface properties of Co-Fe and Fe-Pd liquid alloys, J. Non-Cry. Solid, **394–395**(2014)9–15. https://doi.org/10.1016/j.jnoncrysol.2014.04.001

[22] R. Hultgren, R. L. Orr, P. D. Anderson, K. K. Kelley, Selected values of the thermodynamic properties of binary alloys, 1963, Wiley.

[23] C. H. P. Lupis, J. F. Elliott, Correlation Between Excess Entropy and Enthalpy Functions, Trans. Metall. Soc. AIME, **236**(1966) 130–130.

[24] G. Kaptay, On the tendency of Solutions to Tend Toward Ideal Solutions at High Temperatures, Metal. Mat. Trans. A, **43A**(2012) 531–543. https://doi.org/10.1007/s11661-011-0902-x
[25] H. Fukuyama, M. Watanabe, M. Adachi, Recent studies on thermophysical properties of metallic alloys with PROSPECT: Excess properties to construct a solution model, High temp. high press., **49**(2020)197–210, 10.32908/hthp.v49.851
[26] M. Adachi, Y. Yamagata, M. Watanabe, S. Hamaya, M. Ohtsuka, H. Fukuyama, Composition dependence of normal spectral emissivity of liquid Ni-Al alloys, **61**(2021) 684–689. https://doi.org/10.2355/isijinternational.ISIJINT-2020-233
[27] M. Watanabe, M. Adachi, H. Fukuyama, Heat capacities and theral conductivities of palladium and titanium melts and correlation between thermal diffusivity and density of states for transition metals in a liquid state, J. Mol. Liq., **324**(2021)115138. https://doi.org/10.1016/j.molliq.2020.115138
[28] M. Watanabe, M. Adachi, M. Uchikoshi, H. Fukuyama, Thermal Conductivities of Fe-Ni Melts Measured by Non-contact Laser Modulation Calorimetry, Met. Mat. Trans. A, **50A**(2019) 3295–3300. https://doi.org/10.1007/s11661-019-05250-9
[29] H. Fukuyama, H. Higashi, H. Yamano, Normal spectral emissivity, specific heat capacity, and thermal conductivity of type 316 austenitic stainless steel containing up to 10 mass% B_4C in a liquid state, J. Nucl. Mat., **568**(2022)153865. https://doi.org/10.1016/j.jnucmat.2022.153865
[30] H. Fukuyama, H. Kobatake, K. Takahashi, I. Minato, T. Tsukada, S. Awaji, Development of modulated laser calorimetry using a solid platinum sphere as a reference, Meas. Sci. Technol., **18**(2007) 2059–2066. https://doi.org/10.1088/0957-0233/18/7/036
[31] T. Tsukada, H. Fukuyama, H. Kobatake, Determination of thermal conductivity and emissivity of electromagnetically levitated high-temperature droplet based on the periodic laser-heating method: theory, Int. J. Heat Mass Transf., **50**(2007) 3054–3061. https://doi.org/10.1016/j.ijheatmasstransfer.2006.12.026
[32] M. Watanabe, Y. Takahashi, S. Imaizumi, Y. Zhao, M. Adachi, M. Ohtsuka, A. Chiba, Y. Koizumi, H. Fukuyama, Thermophysical properties of liquid Co-Cr-Mo alloys measured by electromagnetic levitation in a static magnetic field, Thermochim. Acta, **708**(2021)179119. https://doi.org/10.1016/j.tca.2021.179119
[33] H. Fukuyama, H. Higashi, H. Yamano, Effect of B4C addition on the solidus and liquidus temperatures, density and surface tension of type 316 austenitic stainless steel in the liquid state, J. Nucl. Mat., **554**(2021)153100. https://doi.org/10.1016/j.jnucmat.2021.153100
[34] M. Watanabe, M. Adachi, H. Fukuyama, Normal spectral emissivity and heat capacity at constant pressure of Fe–Ni melts, J. Mat. Sci., **52**(2017) 9850–9858. https://doi.org/10.1007/s10853-017-1122-6
[35] M. Uchikoshi, H. Shibuya, T. Kékesi, K. Miura, M. Isshiki, Mass production of high-purity iron using Anion-exchange separation and plasma arc melting, Met. Mat. Trans. B, **40**(2009) 615–618. https://doi.org/10.1007/s11663-009-9269-4
[36] H. Okamoto, Phase Diagrams of Binary Iron Alloys, Fe-Pd (Iron-Palladium), ASM International, Materials Park OH (1993), pp. 319–325.
[37] H. Kobatake, H. Khosroabadi, H. Fukuyama, Normal Spectral Emissivity Measurement of Liquid Iron and Nickel Using Electromagnetic Levitation in Direct Current Magnetic Field, Met. Mat. Trans. A, **43**(2012) 2466–2472. https://doi.org/10.1007/s11661-012-1101-0
[38] K. Schaefers, M. Rösner-Kuhn, M. G. Frohberg, Concentration dependence of the spectral emissivity of liquid binary metallic alloys, **168**(1995) 997–1007. https://doi.org/10.1007/BF02093478
[39] J. A. Treverton, J. L. Margrave, Levitation calorimetry. IV. The thermodynamic properties of liquid cobalt and palladium, The journal of physical chemistry, **75**(1971) 3737–3740. https://doi.org/10.1021/j100693a018
[40] S. Krishnan, G. P. Hansen, R. H. Hauge, J. L. Margrave, Emissivities and optical constants of electromagnetically levitated liquid metals as functions of temperature and wavelength, High temperature science, **26**(1990) 143–164.
[41] B. Wilthan, C. Cagran, G. Pottlacher, E. Kaschnitz, Normal spectral emissivity at 684.5 nm of the liquid binary system Fe-Ni, Monatshefte für Chemie, **136**(2005) 1971–1976. https://doi.org/10.1007/s00706-005-0387-7

[42] E. Kaschnitz, J. L. McClure, A Cezairliyan, Radiance temperatures (in the wavelength range 530-1500 nm) of iron and cobalt at their melting points by a pulse-heating technique, High temp. high press., **29**(1997) 103–111.
[43] H. Watanabe, M. Susa, H. Fukuyama, K. Nagata, Phase (liquid/solid) dependence of the normal spectral emissivity for iron, cobalt, and nickel at melting point, Int. J. Therm. Phys., **24**(2003) 473–488. https://doi.org/10.1023/A:1022924105951
[44] P. Ratanapupech, R. G. Bautista, Normal spectral emissivities of liquid iron, liquid nickel, and liquid iron-nickel alloys, High temperature science, **14**(1981) 269–283.
[45] T. Mori, K. Fujimura, T. Higashi, H. Yoshimoto, On the emissivities of molten metals and iron alloys, Tetsu to hagane, **57**(1971) 100–114. https://doi.org/10.2355/tetsutohagane1955.57.7_1198
[46] C. C. Bidwell, A comparison of actual and black-body temperatures, Phys. Rev. **3**(1914) 439–449. https://doi.org/10.1103/PhysRev.3.439
[47] M. D. Dastur, N. A. Gokcen, Optical temperature scale and emissivity of liquid iron, Met. Trans., **185**(1949) 665–667.
[48] K. W. Lange, H. Schenck, Messung des spektralen emissionsgrades von metallen und metallegierungen, Archiv für das eisenhüttenwesen, **39**(1968) 611–615.
[49] K. Morohoshi, Tohoku University, (2012), Ph. D. thesis.
[50] M. Uchikoshi, M. Isshiki, H. Fukuyama, Surface tension of liquid iron as functions of oxygen activity and temperature, ISIJ int., **51**(2011) 1580–1586. https://doi.org/10.2355/isijinternational.51.1580
[51] Y. S. Touloukian, D. P. Dewitt, Thermophysical properties of matter-The TPRC Data Series vol. 8. Thermal radiative properties-Nonmetallic solids, (1972).
[52] G. R. Blair, Determination of spectral emissivity of ceramic bodies at elevated temperatures, Journal of the American ceramic society, **43**(1960) 197–203. https://doi.org/10.1111/j.1151-2916.1960.tb12981.x
[53] G. Wilde, G. P. Görler, R. Willnecker, The specific heat of highly undercooled (Co, Ni, Fe)-Pd melts, J. Non-Cry. Sol., **205–207**(1996) 317–321. https://doi.org/10.1016/S0022-3093(96)00247-5
[54] G. Wilde, G. P. Görler, R. Willnecker, Specific heat capacity of undercooled magnetic melts, Appl. Phys. Let., **68**(1996) 2953–2955. https://doi.org/10.1063/1.116366
[55] G. Wilde, G. P. Görler, R. Willnecker, Hypercooling of completely miscible alloys, Appl. Phys. Let., **69**(1996) 2995–2997. https://doi.org/10.1063/1.117755
[56] W. Schnelle, J. Engelhardt, E. Gmelin, Specific heat capacity of Apiezon N high vacuum grease and of Duran borosilicate glass, Cryogenics, **39**(1999) 271–275. https://doi.org/10.1016/S0011-2275(99)00035-1
[57] P. Richet, M. A. Bouhifd, P. Courtial, C. Tequi, Configurational heat capacity and entropy of borosilicate melts, J. Non-Cry. Sol., **211**(1997) 271–280. https://doi.org/10.1016/S0022-3093(96)00646-1
[58] Evaluation of measurement data-Guide to the expression of uncertainty in measurement, JCGM **100**(2008).
[59] M. Hayashi, M. Murata, H. Fukuyama, K. Nagata, Normal spectral emissivities of liquid Ag-Cu alloys in the visible and infrared regions, Metall. Mat. Trans. B, **33**(2002) 47–54. https://doi.org/10.1007/s11663-002-0084-4
[60] M. Beutl, G. Pottlacher, H. Jäger, Thermophysical Properties of Liquid Iron, Int. J. Therm., **15**(1994) 1323–1331. https://doi.org/10.1007/BF01458840
[61] E. Esposito, H. Ehrenreich, C. D. Gelatt, Jr., Electrical transport in transition-metal liquids and metallic glasses, Phys. Rev. B, **18**(1978) 3913–3920. https://doi.org/10.1103/PhysRevB.18.3913